I&EC research
Industrial & Engineering Chemistry Research

Article

pubs.acs.org/IECR

Graphene Oxide-Impregnated PVA–STA Composite Polymer Electrolyte Membrane Separator for Power Generation in a Single-Chambered Microbial Fuel Cell

Santimoy Khilari,[†,‡] Soumya Pandit,[‡,§] Makarand M. Ghangrekar,[∥] Debabrata Pradhan,[†] and Debabrata Das*[,§]

[†]Materials Science Centre, [§]Department of Biotechnology, and [∥]Department of Civil Engineering, Indian Institute of Technology Kharagpur, Kharagpur-721302, India

Supporting Information

ABSTRACT: The present study deals with the development and application of a proton-exchange polymer membrane separator consisting of graphene oxide (GO), poly(vinyl alcohol) (PVA), and silicotungstic acid (STA) in a single-chambered microbial fuel cell (sMFC). GO and the prepared membranes were characterized by FT-IR spectroscopy, XRD, SEM, TEM, and AC impedance analysis. Higher power was achieved with a 0.5 wt % GO-incorporated PVA–STA–GO membrane compared to a Nafion 117 membrane. The effects of oxygen crossover and membrane-cathode-assembly (MCA) area were evaluated in terms of current density and Coulombic efficiency. The electrochemical behavior of the membrane in an MFC was improved by adding different amounts of GO to the membrane to reduce biofouling and also to enhance proton conductivity. A maximum power density of 1.9 W/m^3 was obtained when acetate wastewater was treated in an sMFC equipped with a PVA–STA–GO-based MCA. Therefore, PVA–STA–GO could be utilized as an efficient and inexpensive separator for sMFCs.

1. INTRODUCTION

Microbial fuel cells (MFCs) have the capability of converting biodegradable materials into electricity. MFCs involve a biochemical-catalyzed process using electrochemically active bacteria (EAB) that can oxidize any biodegradable organic matter and transfer electrons to an electrode.[1−3] MFCs are gaining popularity as a promising alternate technology for harvesting electricity through wastewater treatment, thus allowing renewable energy production from an abundant and inexpensive source.[4−6] To make MFCs economically viable, it is necessary to reduce the manufacturing costs by simplifying the design to achieve enhanced volumetric power density along with Coulombic efficiency (CE).[7]

In recent years, significant efforts have been made to improve MFC performance through various engineering approaches, among which the separator technology associated with MFCs is of great importance and has attracted considerable interest.[8,9] In MFCs, membranes are mainly used as separators to prevent the anolyte from reaching the cathode, although membrane-less MFCs have been reported and found to be promising because of their low cost, simple configuration, and relatively high power density at a small scale. In the absence of a membrane, however, oxygen and substrate diffusion would increase, decreasing the CE and the catalytic activity of the EAB and making the MFC operation less efficient. In addition, the electrode spacing in a membrane-less MFC is limited to a certain range (about 2−4 cm), which contributes to the risk of a short circuit. Furthermore, there is a limit on the design of membrane-less MFCs such as flat-plate and tubular MFCs.[10,11] Therefore, it is widely recognized that a membrane is necessary to ensure efficient and sustainable MFC operation. Earlier published reports suggest that the challenges of using membranes in MFCs include (1) the manufacturing costs of the membrane, (2) the internal resistance of the membrane, and (3) biofouling on the membrane during MFC operation.[9]

Proton conduction from the anode to the cathode compartment is affected by the properties of the proton-exchange membrane (PEM). Solid polymer electrolyte membranes have been used extensively as PEMs in conventional chemical fuel cells not only because of their high ionic conductivity but also because of their thermal and mechanical stability. Until now, sulfonated cation-exchange membranes, mostly Nafion, have been used for the preparation of membrane electrode assemblies because of the high selective permeability of Nafion to protons.[12] However, the high cost and difficulties in the synthesis and processing of Nafion limit it for the scaling up of MFCs.[13] Biofouling has also been reported for Nafion 117, which adds to the operation and maintenance cost.[14] Oxygen leakage from the cathode to the anode and substrate loss are additional problems associated with Nafion as the cation-exchange membrane (CEM).[15] Therefore, there is an urgent need to develop low-cost membranes for scaling up MFCs and creating affordable treatment systems considering the previously mentioned bottlenecks.

Polymer electrolyte membranes have received considerable attention from the scientific community for providing alternatives to Nafion membranes in fuel cell technology.[16] Recently, poly(vinyl alcohol)- (PVA-) based polymer electrolyte membranes have drawn the interest of researchers for their

Received: May 20, 2013
Revised: July 8, 2013
Accepted: July 18, 2013
Published: July 18, 2013

dx.doi.org/10.1021/ie4016045 | *Ind. Eng. Chem. Res.* 2013, 52, 11597−11606

broad applications in fuel cells, pervaporation, proton exchange, and so on.[17,18] Low-cost PVA−inorganic composite membranes show excellent dimensional and thermal stabilities, good mechanical stability, controllable physical properties, and good hydrophilic and electrochemical properties, all of which are essential for ion-exchange membranes.[18] The ion-transport properties of polymeric membranes can be improved by the addition of inorganic dopants. Heteropolyacids (HPAs) such as phosphomolybdic acid (PMA), silicotungstic acid (STA), and phosphotungstic acid (PTA) are widely used for such doping during polymer electrolyte preparation, where the polyanions act as ion carriers. The presence of considerable numbers of water molecules in the crystal structures of HPAs offers high proton conductivity. Therefore, the HPA content in a membrane is the most critical aspect determining the performance of the membrane.[19] To obtain better conductivity and stability, optimization of the HPA content is needed. In the present study, a specific amount of STA (30 wt %) was incorporated into PVA-based membranes, as reported elsewhere.[18] It was also reported that the conductivity of such membranes prepared with 30 wt % STA is lower than that of Nafion 117 membranes.[18] Further, the addition of an ion-conductive filler to the membrane has the ability to improve its conductivity.[20] Graphene oxide (GO) is a two-dimensional single-layered homologue of graphene containing various oxygen functional groups (e.g., hydroxyl, epoxide, carbonyl, carboxyl) that has wide application in supercapacitiors, photovoltaic devices, biosensors, and so on. The incorporation of GO into a polymer matrix improves many of its physical and chemical properties, including ion conductivity and mechanical strength.[20,21] It was therefore hypothesized that the incorporation of GO into the polymer matrix could improve the conductivity of polymer electrolyte membranes and reduce biofouling on the membranes, which could lead to enhanced power generation and higher power densities in single-chambered microbial fuel cells (sMFCs).[22,23]

Therefore, the aim of the present study was to determine the suitability of PVA−STA-based membranes in an MFC as a low-cost separator. In the present study, we report the synthesis and characterization of PVA−STA−GO membranes, as well as a comparison of their performance with that of Nafion 117 as the separator in an sMFC. The oxygen crossover of both types of membranes was measured using a dissolved oxygen probe. The performances of sMFCs with membrane cathode assemblies (MCAs) of different sizes are reported in terms of power output. Additionally, the effects of different GO loadings on the current generation and biofouling of the membranes was investigated.

2. MATERIALS AND METHODS

2.1. Preparation of PVA−STA and PVA−STA−GO Membranes. PVA−STA membranes were prepared as suggested by Anis et al., using the solution casting method.[18] To prepare the membranes, 5% (w/v) PVA solution was obtained by dissolving the required amount of PVA in distilled water at 80 °C with constant stirring. Then, 30 wt % STA was added to 20 mL of the as-prepared PVA solution, and the mixture was stirred for a few minutes to form a homogeneous solution. Next, 2 mL of 1.0% (v/v) glutaraldehyde was added to this mixture, and the resulting solution was stirred for 2−3 min. Finally, the solution was cast in a Petri dish and allowed to dry at 50 °C in an oven. After drying, the thin film was peeled off from the Petri dish and is denoted as membrane M1.

GO was synthesized from graphite powder using a modified Hummers method with $KMnO_4$ and H_2SO_4 as the oxidizing agents.[24] For purification, the product was washed 6−8 times with 5% (v/v) HCl solution followed by deionized H_2O. GO powder obtained in this way was used to prepare GO-modified PVA−STA membranes. For each PVA−STA−GO membrane, the required amount (0.3, 0.5, and 0.9 wt %) of GO powder was dispersed in 20 mL of distilled water by sonication for 2 h in a sonicator. The GO-dispersed solution was then added to 20 mL of a PVA−STA mixture prepared as in the preceding paragraph with constant stirring for 10 min. After that, 2 mL of 1.0% glutaraldehyde was added to the solution, and the solution was cast in a Petri dish, which was placed in an oven and dried at 50 °C. After drying, the thin film was peeled off from the Petri dish. The composites obtained in this way with different weight percentages of GO are denoted as membranes M2 (0.3 wt % GO), M3 (0.5 wt % GO), and M4 (0.9 wt % GO). All of the membranes had thicknesses of 100 ± 5 μm.

2.2. Physical Characterization of GO and Composite Membranes. The as-synthesized GO and as-prepared membranes were characterized by X-ray diffraction (XRD) with a Rigaku Ultima III X-ray diffractometer (Cu Kα radiation). The microstructure of GO was analyzed by transmission electron microscopy (TEM) in an FEI Tecnai G2 20S Twin transmission electron microscope operated at 200 kV accelerating voltage. The cross-sectional features of the as-prepared membrane were studied with a Zeiss scanning electron microscope operated at 20 kV. Elemental analysis of the membrane was performed with an Oxford Inca energy-dispersive X-ray (EDX) analyzer attached to scanning electron microscopy (SEM) instrument. Fourier transform infrared (FT-IR) spectra of the prepared membranes were recorded on a Bruker Tensor-27 FT-IR spectrophotometer operated in transmittance mode in the wavenumber range from 4000 to 400 cm^{-1}. The proton conductivity of the membranes was investigated by AC impedance analysis in a HIOKI 35-3250 inductance−capacitance−resistance (LCR) meter. During measurements, a piece of membrane was placed in a homemade conductivity cell, and AC impedance was measured under a 10 mV oscillating potential over the frequency range from 10 Hz to 2 MHz. The mechanical properties of the prepared membranes were studied in terms of tensile strength and percentage elongation measurements. The tensile strength and percentage elongation at break of the prepared membranes were measured in a Tinius Olsen universal testing machine. The universal testing machine was operated at a crosshead speed of 12.5 mm/min at 30 °C. The dimensions of the test samples were 80 mm × 15 mm, and each sample was tested three times. The average of the three measurements was considered.

2.3. Preparation of Membrane Cathode Assembly. Carbon cloth was used as the cathode (round sheet, effective diameter of 3 cm unless stated otherwise). To prepare ink containing cathode catalyst, 0.1 mg/cm^2 Pt/C dust (20 wt % Pt/C, Sigma-Aldrich) and carbon black Vulcan XC-72 (3 mg/cm^2; Cabot Corp., Tamil Nadu, India) were taken in 20 mL of 1:1 acetone/isopropyl alcohol solution with 1.2 μL of PVA (1% w/v) aqueous solution as the binder. Ultrasonication of the PVA−Pt/C aqueous/acetone/isopropyl alcohol was performed for 30 min, and the resulting mixture was used as ink to spread the cathode. Ink containing cathode catalyst was sprayed on the carbon cloth, which was then kept in an oven heated at 60 °C. The membrane cathode assembly (MCA) was manufactured by bonding the membrane (PVA–STA–GO) directly onto a flexible carbon cloth electrode containing Pt catalyst through hot-pressing at 85 °C for 5 min (Moore Max Ton Hydraulic Press, 800 kPa). Nafion 117 (DuPont, Wilmington, DE) was used to compare the performance of PVA–STA and PVA–STA–GO (both membranes M1 and M3). The same size sample of Nafion was sequentially boiled in H_2O_2 (30%), deionized water, 0.5 M H_2SO_4, and deionized water (each time for 1 h). The carbon cloth was coated with 0.1 mg/cm^2 Pt/C and a Nafion (5%, DuPont) binder on the water-facing side. The PEM was then hot-pressed directly onto the carbon cloth by heating it to 140 °C at 1.5 MPa for 5 min.

2.4. MFC Configuration. Three identical cylindrical-type sMFCs were used for experiments. Borosil glass bottles of 500 mL capacity (empty anode chamber) with a side opening (diameter = 3 cm) were connected at the bottom (Figure S1, Supporting Information). A hot-pressed membrane cathode assembly (7.07 cm^2, 3-cm diameter) consisting of a PVA–STA–GO membrane with a catalyst-loaded carbon cloth was clamped with the flange of the opening side; the electrode spacing between the anode and cathode was 4 cm. The MFC consisted of an anode and the MCA placed on opposite sides. The anode electrodes were made of carbon cloth (6 × 4 cm^2) and did not contain any catalyst. The effective anolyte volume was 350 mL, and a comparative study was performed in terms of bioelectricity generation using three different membranes, namely, Nafion, native PVA–STA (membrane M1) and PVA–STA–GO (GO content = 0.5 wt %, membrane M3) in sMFCs with the same configuration. The effects of blending different amounts of GO in the PVA–STA–GO membranes on the performance of the sMFC were also investigated. Further, to determine the effect of the projected surface area of the MCA, three Borosil glass bottles of 500 mL capacity (empty anode chamber) with different side openings (diameters of 2, 3, and 4.8 cm) were used.

To carry out an oxygen mass-transfer study as well as biofouling experiments, a dual-chambered MFC was used. The dual-chambered MFC setup comprised two fabricated glass compartments of 500 mL capacity with a side opening at the bottom (28 cm^2). The two chambers were clamped when a PEM (PVA–STA–GO or Nafion 117) was used. Carbon cloth of 6 × 4 cm^2 area was used as the anode electrode, whereas a platinum-coated tantalum electrode (dimensions = 3 × 5 cm^2; Titanium Tantalum Products Ltd., Chennai, India) was used as the cathode. The cathode chamber contained 350 mL of phosphate-buffered saline (PBS; 50 mM, pH 7.0) with continuous aeration. Other configuration and operating parameters were the same as for the single-chambered MFC.

2.5. Analyte and Inoculum. A synthetic wastewater containing acetate as the carbon source was used throughout the study, according to the composition provided in ref 25. The chemical oxygen demand (COD) of synthetic acetate wastewater was in the range of 4.99–5.01 g/L for all of the MFCs. The initial pH in all of the MFCs was maintained in the range of 7.0 ± 0.02. Anaerobic mixed consortia obtained from the bottom sludge of a septic tank of Indian Institute of Technology (IIT) Kharagpur was used as the parent inoculum. The inoculum sludge was sieved through a 1-mm sieve, preheated at 100 °C for 15 min, and allowed to cool. Prior to inoculation, the mixed culture was washed three times in saline buffer (5000 rpm) and enriched in designed synthetic wastewater (DSW) under an anaerobic microenvironment at pH 7 (100 rpm, room temperature, 48 h). The resulting enriched culture was inoculated along with feed (inoculum concentration = 2.8 g of volatile suspended solids/L). The MFC was operated in batch mode; prior to startup, the anodic compartment was inoculated with pretreated mixed microflora. Multiple cycles were carried out. Each batch cycle time was 48 h. After every feeding event, the MFC was sparged with oxygen-free N_2 for 2 min to maintain an anaerobic microenvironment. Prior to feeding, the pH of wastewater was adjusted to desire pH value of 7.0.

2.6. Analytical Measurements and Calculations. The performance of the MFCs was examined in terms of power generation and Coulombic efficiency. Detailed measurement and calculation techniques for electrode potentials, power, power density, and Coulombic efficiency determination are described in the Supporting Information. Oxygen mass-transfer coefficient for the PVA–STA–GO membrane was calculated according to the method described by Kim et al.[13] and Lefebvre et al.[26] The oxygen mass-transfer coefficient (k_{cm}, cm/s) was measured in an uninoculated dual-chambered reactor that was mixed with a magnetic stir bar. The two chambers of the reactor were separated by a partition on which PVA–STA–GO membrane M3 (8 cm × 8 cm) was fixed. Both chambers of the reactor were filled with 50 mM phosphate buffer solution containing (per liter in deionized water, pH 7): 0.31 g of NH_4Cl, 0.13 g of KCl, 2.69 g of $NaH_2PO_4 \cdot H_2O$, and 4.33 g of Na_2HPO_4. Before the measurement of k_{cm}, the dissolved oxygen (DO) of the anode chamber was eliminated by purging with N_2 gas. During k_{cm} measurements, the DO in the cathode chamber was maintained saturated through the continuous supply of air using an aquarium pump (2 L/min). The DO of the anode chamber was monitored using a DO meter (Mettler Toledo, Pro 6800). The DO probe was connected to a data-logging system, and DO concentration was recorded in intervals of 15 min for a batch time of 48 h using the data-logger software. The diffusion coefficient (D_{cm}, cm^2/s) was calculated using the equation

$$D_{cm} = \frac{-VL_t}{2At} \ln\left(\frac{C_{1,0} - C_2}{C_{1,0}}\right) \tag{1}$$

where V is the liquid volume of each chamber, L_t is the membrane thickness, A is the membrane cross-sectional area, t is the batch time, $C_{1,0}$ is the saturated oxygen concentration in the chamber determined by the DO probe, and C_2 is the DO in the other chamber at time t. The oxygen transfer coefficient (k_{cm}, cm/s) was calculated as

$$k_{cm} = D_{cm}/L_t \tag{2}$$

Short-circuit currents (I_{sc}) were measured with a Mastech 6000 counts digital multimeter (Precision Mastech Enterprises Co., Hong Kong) when the anode and cathode were connected directly through the multimeter. The internal resistance of the MFCs was calculated by the current-interrupt method.[27] While in closed-circuit mode, once the MFC was producing a stable current output (I) and potential (V), the circuit was opened, causing a steep initial rise in the cell voltage (V_R), followed by gradual further increment. The steep rise is attributed to ohmic losses caused by the internal resistance (R_{int}) of the MFC and can hence be calculated as

$$R_{int} = \frac{V_R}{I} \tag{3}$$

The volatile fatty acids (VFAs) were determined using a gas chromatograph (Agilent Technologies, Palo Alto, CA) equipped with a flame ionization detector (FID). The COD values of the anolyte were measured according to American Public Health Association (APHA) standard methods using a COD measurement instrument set (DRB200 and DR2800 portable spectrophotometer, HACH, Loveland, CO). The pH values were monitored using a desktop pH meter (pH 510, Cyberscan, Singapore). The Lowry method was used to measure the protein content attached to the membrane.[28] Membranes were collected after 76 days of MFC operation and kept in an autoclave with 20 mM phosphate buffer, after which the attached material was scratched from the membrane surface and suspended for 20 min in 10 mL of lysis buffer in a Falcon tube to facilitate the extraction of proteins.[29] An aliquot of this well-mixed suspension was diluted with the lysis buffer; 0.1 mL of this diluted suspension was taken, the same amount of sodium dodecyl sulfate (SDS) solution was added, and the mixture was vortexed. Folin reagent was added, and the mixture was immediately vortexed. After 30 min, the absorbance of the sample was measured at a wavelength of 750 nm in a Perkin-Elmer Lambda 25 spectrophotometer.

3. RESULTS AND DISCUSSION

3.1. Characterization of the Composite Membrane.

FT-IR Spectroscopy. FT-IR spectra of GO and the prepared membranes were recorded on a Bruker FT-IR spectrophotometer in transmittance mode by scanning from 4000 to 400 cm^{-1}. Figure 1 shows the recorded FT-IR spectra. The infrared spectrum of GO consisted of well-defined peaks for the C—O vibrations of epoxy groups at 1130 cm^{-1}, the C—OH stretching vibration at 1230 cm^{-1}, and the C═O stretching vibrations of carbonyl and carboxylic groups at 1720 cm^{-1}. The absorption peak at 1618 cm^{-1} was due to the aromatic carbon double-bond vibration. A broad band observed at 3390 cm^{-1} in the FT-IR spectrum is attributed to the stretching vibration of —OH groups and adsorbed water molecules.[30] Several strong absorptions were observed below 1100 cm^{-1} for polyoxymetalates in both PVA−STA and PVA−STA−GO membranes. Absorption bands at 972, 919, 843, and 786 cm^{-1} were assigned to stretching vibrations of W—O$_d$—W, Si—O$_a$—W, W—O$_b$—W, and W—O$_c$—W bonds, respectively.[19] Shifts in the band positions were noted as a result of the presence of Coulombic interactions between donor (organic composite) and acceptor (HPA) species. These interactions depend on the amount of HPA introduced in the composite.[31] Cross-linking produced C—O—C bonds, which showed a characteristic absorption at 1138 cm^{-1}. The absorption peak at 1709 cm^{-1} was due to the aldehyde C═O stretching of glutaraldehyde. The GO-modified PVA−STA membranes shows the characteristic signatures of both cross-linked PVA−STA polymer electrolyte and GO. The intensity of the peaks appearing near 1700 cm^{-1} increased in the GO-modified membranes because of the presence of the carbonyl groups of GO.

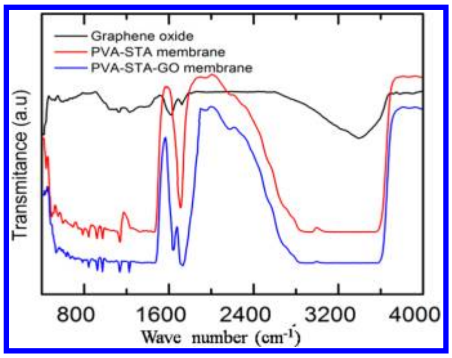

Figure 1. FT-IR spectra of GO, PVA−STA, and PVA−STA−GO membranes.

XRD. X-ray diffraction analysis of GO and two membranes (M1 and M2) was performed, and the results are shown in Figure 2. The synthesized GO showed a characteristic peak at 11.9° corresponding to the (001) plane of GO with an interplanar spacing of 7.43 Å. [32] The *d* spacing of the (001) plane of GO (7.43 Å) is far higher than that of the precursor graphite (6.8 Å). The interlayer spacing is far higher than that of pristine graphite, which indicates the incorporation of oxygen functionalities on the graphite planes. The PVA−STA composite membrane showed a broad peak at 19.7°, indicating the presence of PVA in the membrane. Broadening of the peak was attributed to a reduction in the crystallinity of pristine PVA (semicrystalline) due to cross-linking and ester formation with STA.[33] Also, the addition of STA reduced the crystallinity of the PVA membrane and shifted the peak to a lower value. In the case of GO-modified membranes, a peak at 18.7° was found along with another peak below 10° for GO incorporation. It is important to note that the diffraction feature of GO was changed in the PVA−STA−GO membranes. The (001) reflection of GO was shifted to lower 2θ value (8.8°), which indicates that PVA molecules were intercalated into the GO layers and increased the interplanar spacing between the GO layers.[34] This intercalation of PVA suggests that the GO was well-distributed in the polymer matrix.

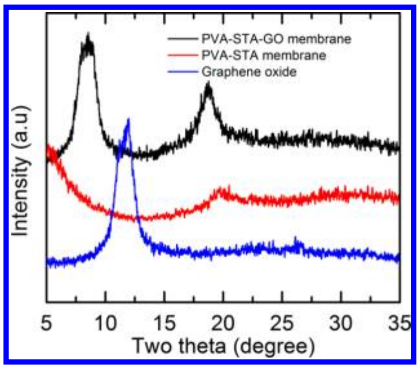

Figure 2. XRD patterns of GO powder and PVA−STA and PVA−STA−GO composite membranes.

SEM AND EDX Spectroscopy. The cross-sectional morphologies of the as-prepared membranes were studied in a Zeiss scanning electron microscope operated at 20 kV. Panels a,b and c,d of Figure 3 show cross-sectional SEM micrographs of PVA−STA and PVA−STA−GO membranes, respectively. The PVA−STA membrane appears to be compact and smooth. In contrast, the PVA−STA−GO membrane appears to have a fibrillar morphology (Figure 3c). A magnified image of the PVA−STA−GO membrane (Figure 3d) shows the morphology of GO sheets, suggesting the distribution of GO in the polymer matrix. Energy-dispersive X-ray analysis shows the presence of silicon, tungsten, oxygen, and carbon, indicating the presence of silicotungstic acid in the PVA−STA−GO membrane (Figure 3e).

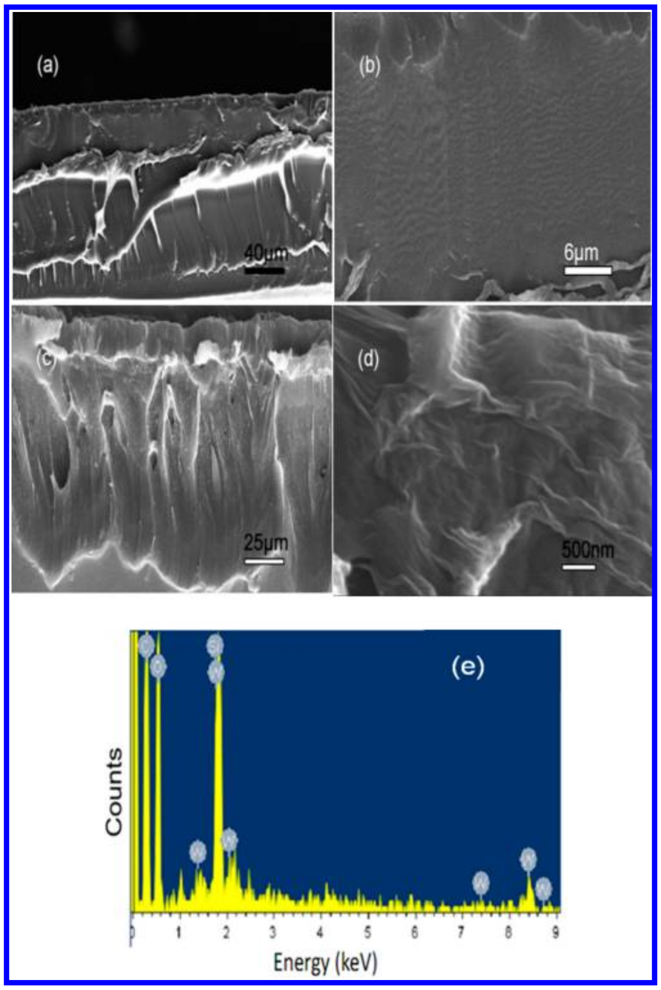

Figure 3. Cross-sectional SEM images of (a,b) PVA−STA and (c,d) PVA−STA−GO membranes. (e) EDX spectrum of the PVA−STA−GO membrane.

TEM. The microstructure of the prepared GO was investigated by bright-field TEM analysis, and the results are shown in Figure 4a. The TEM image of the prepared GO shows a thin sheetlike two-dimensional structure (flakes). Some of the GO sheets had a crumpled microstructure, which might be due to the presence of oxygen functionalities in the GO sheets. A selected-area electron diffraction (SAED) pattern obtained from a sheet showed a ring consisting of some diffraction spots. This indicates that the GO sheets were not completely amorphous, as some short-range order was present. The lack of a hexagonal bright diffraction of graphite in the obtained SAED pattern confirms that the sheets were GO (Figure 4b). Because of the presence of oxygen functionalities, a higher number of spots appeared in the SAED pattern of the GO sheet.

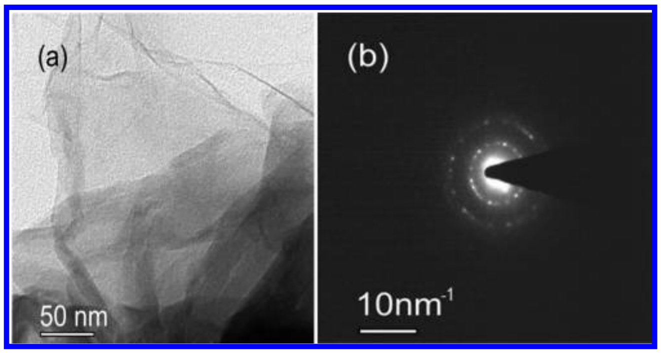

Figure 4. (a) TEM image of GO and (b) SAED pattern of GO sheets.

Proton Conductivity. The proton conductivities of the membranes were investigated by AC impedance analysis over the frequency range from 10 Hz to 2 MHz under a 10 mV oscillating potential. Figure 5 shows the complex impedance plots of different as-synthesized membranes at 35 °C. Prior to the impedance measurements, each sample was immersed in deionized water (18 Ω) for at least 12 h at room temperature to become hydrated. A hydrated membrane sample of dimensions 1.5 cm × 2 cm was placed between two platinum electrodes of a homemade conductivity cell and clamped. The measurement was carried out by exposing the membrane between the two electrodes in deionized water to maintain the relative humidity at 100%. Detailed descriptions of the conductivity cell and measuring procedure were reported by Wang et al.[35] The conductivity of the membranes was determined as

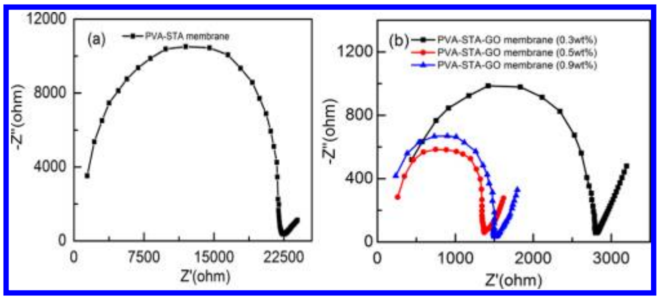

Figure 5. Complex impedance plots of (a) a PVA−STA membrane and (b) three PVA−STA−GO membranes with different GO contents.

$$\sigma = \frac{l}{Rdw} \tag{4}$$

where l, R, d, and w represent the distance between the electrodes and the resistance, thickness, and width of the membrane, respectively. Resistance (R) was measured from the low intersect of the semicircle with the real (Z) axis in the high-frequency region in the complex impedance plot. PVA−STA composite membrane showed a conductivity of 4.6×10^{-3} S cm^{-1}, whereas the GO-modified membranes showed conductivities of 3.5×10^{-2}, 7.2×10^{-2}, and 6.5×10^{-2} S cm^{-1} for 0.3, 0.5, and 0.9 wt % GO (membranes M2−M4), respectively. Ion-exchange membranes in MFCs produce transmembrane potentials that contribute significantly toward ohmic losses and can be minimized by using membranes of low resistivity. A 7.6-fold increase in ionic conductivity was recorded upon the incorporation of 0.3 wt % GO in a PVA−STA membrane (M2) as compared to a native PVA−STA membrane without GO (membrane M1). This improvement in proton conductivity comes from an increase in the number of ion-exchange groups (—COOH groups of GO), along with an increase in the interconnected transfer channels in the presence of GO. However, the proton conductivity of membrane M2 (0.3 wt % GO) was found to be less than that of a Nafion 117 membrane (6.2×10^{-2} S cm^{-1}). A further increment in the GO loading (0.5 wt %) increased the conductivity above that of Nafion 117. However, the proton conductivity of the PVA−STA−GO membranes increased up to a certain GO loading, after which it decreased with a further increase in GO content. Specifically, the proton conductivity decreased to 10% when 0.9 wt % GO was incorporated instead of 0.5 wt % GO. This decrease in conductivity can be attributed to the "blocking effect" of filler loading.[20]

Mechanical Property: Tensile Strength. Unlike in a conventional fuel cell, the membrane (separator) in an MFC has to withstand a high hydrostatic pressure. Therefore, the membrane must have good mechanical strength to sustain the hydrostatic pressure. Generally, the mechanical strength of membranes is studied by tensile strength measurements. To determine the suitability of PVA–STA-based membranes as MFC separators, tensile strength measurements were performed. The higher the tensile strength, the better the mechanical stability of a membrane. The tensile strength of un-cross-linked pristine PVA membrane was found to be 22.3 MPa, lower than that of the cross-linked PVA membrane (31.1 MPa). In fact, cross-linking reduces the mobility of polymer chain and forms good interconnections between the polymer chains, leading to the improved mechanical strength and increased tensile strength of the cross-linked PVA membrane. The addition of STA to the PVA matrix (cross-linked) increased the tensile strength of the composite membrane slightly to 31.3 MPa. In contrast, the incorporation of GO increased the tensile strength significantly to 39.1 MPa (0.3 wt %), which is higher than the tensile strength of Nafion 117 (37 MPa).[20] Further increases in the GO content of the PVA–STA matrix significantly improved the tensile strength of the composite membranes (45.98 and 58.25 MPa for 0.5 and 0.9 wt % GO loadings, respectively). In the GO-incorporated composite membranes, GO acts as a filler in the composite membrane that strongly adheres to the interface and makes an interlocking structure between the polymer (PVA) and GO. This interaction is responsible for the high tensile strength of PVA–STA–GO membranes. The percentage elongation at break increased upon addition of STA mainly due to the presence of acid formed ester and reduced hydrogen bonding in the PVA matrix.[18] Further, the addition of GO to the PVA–STA matrix caused the elongation at break to decrease significantly. Thus, the GO-modified membranes showed good mechanical stability. This study signifies the usefulness of GO-blended PVA–STA-based membranes as MFC separators.

3.2. Performance of PVA–STA Membranes in an sMFC and Comparative Study with Nafion 117.

Oxygen Mass Transfer. The oxygen crossover from cathode to anode through the Nafion 117 PVA–STA and PVA–STA–GO membranes (0.5 wt % GO) was evaluated using uninoculated MFC reactors. A dual-chambered MFC containing the medium solution was initially sparged with nitrogen gas to remove dissolved oxygen. DO accumulation measurements were made in a sterile medium solution in the anode over a period of 10 h by placing the DO probe on top of the two-chambered MFC. The DO concentration of the Nafion 117 membrane was found to increase from 0.1 to 1.034 mg/L after 8 h due to oxygen transfer across the membrane. In contrast, in the same time period of 8 h, the DO concentration in the case of the PVA–STA–GO membrane increased from 0.1 to 0.37 mg/L. Therefore, the oxygen mass-transfer coefficient (k_{cm}) and oxygen diffusion coefficient (D_{cm}) were estimated to be 2.8 × 10^{-5} cm/s, and 4.2 × 10^{-7} cm^2/s, respectively, for the Nafion 117 membrane and k_{cm} = 6.1 × 10^{-6} cm/s and D_{cm} = 5.7 × 10^{-8} cm^2/s, respectively, for the PVA–STA membrane. Further, it was observed that a change in the STA content in the PVA–STA polymer electrolyte had no significant effect on oxygen permeation. MFCs with different PVA–STA–GO membranes (M2–M4) were found to have values of k_{cm} = 2.2 × 10^{-6}, 1.4 × 10^{-6}, and 1.1 × 10^{-6} cm/s, respectively, and D_{cm} = 2.4 × 10^{-8}, 1.5 × 10^{-8}, and 1.05 × 10^{-8} cm^2/s, respectively, which are significantly lower than the corresponding values for the Nafion 117 membrane. The oxygen permeability decreased upon the incorporation of GO into the PVA–STA polymer electrolyte because of the gas barrier properties of GO. It was observed that the increase in GO content decreased the oxygen permeability. The platelike two-dimensional GO sheets were well-dispersed in the polymer matrix and increased the tortuous diffusion paths, resulting in lowered oxygen diffusion.[36]

Voltage Generation. Under the batch mode of operation, for a feed cycle time of 48 h, all three sMFCs investigated, namely, those using Nafion 117, PVA–STA, and PVA–STA–GO (0.5 wt % GO) membranes, took a period of 2 weeks to reach stable conditions. A slow increase in current was observed with duration of operation. At a 100 Ω external load, the current production reached maximum values of 1.76, 1.68, and 2.04 mA, respectively, on the 16th day of sMFC operation. Stable power was generated after seven sequential transfers of acetate medium into the anode chamber of the mediator-less sMFCs. For the sMFCs with Nafion, PVA–STA, and PVA–STA–GO membranes, maximum sustainable current densities (normalized to analyte volume) of 5.02, 4.84, and 6.0 A/m^3, respectively, were generated with corresponding maximum operating voltages of 0.176, 0.17, and 0.21 V (Figure 6). However, gradual reductions in current and voltage were observed over the period of operation even when substrate was provided for the sMFC with the Nafion membrane.

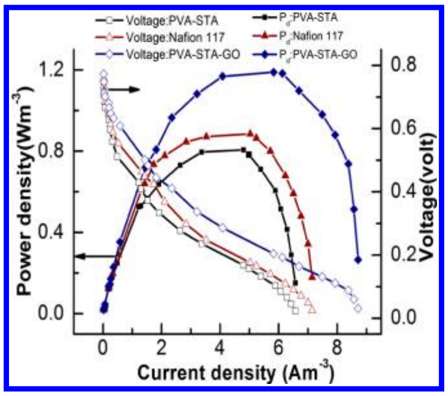

Figure 6. Comparison of polarization results for MFCs using Nafion 117, PVA–STA, and PVA–STA–GO membranes.

Polarization Study. Periodically recording polarization curves allows the monitoring of the evolution of the (a) maximum current, (b) power generation, and (c) electrochemical properties of the anode compartment. The height of the polarization curves is related to the overall performance of the MFC, whereas the shape is related to the presence of different types of polarizations or losses. Polarization curves were obtained after nine batch cycles by varying the external resistance of the closed circuit using a variable resistance box (range from 90 kΩ to 10 Ω) in discrete steps and measuring the corresponding voltage drop. The average time required for obtaining a stable reading was 15–20 min. The power densities obtained showed that PVA–STA–GO membrane M3 (0.5 wt % GO) produced a high volumetric power density of 1.19 W/m^3. The electricity output of the MFC using the Nafion membrane was 64.5 mW/m^2 at a current density of 366.6 mA/m^2, whereas the values were 86.7 mW/m^2 at a current density of 425 mA/m^2 and 58.8 mW/m^2 at a current density of 350 mA/m^2 for the PVA–STA–GO and PVA–STA membranes, respectively (normalized to anode surface area; see eq 3 of the Supporting Information). Maximum volumetric power densities of 0.88 and 0.80 W/m^3 were achieved using the Nafion and PVA–STA membranes, respectively, which were 26% and 32% lower than that obtained with the PVA–STA–GO-membrane-based sMFC (Figure 6). These results clearly indicate that PVA–STA–GO provided better power generation. This finding can be attributed to the 1-order-of-magnitude lower oxygen permeation of PVA–STA–GO compared to Nafion 117. Oxygen diffusion from the cathode to the anode chamber through the separator reduces the efficiency of the MFC because part of the substrate is consumed directly by the oxygen rather than through the transfer of electrons though the electrode and the circuit. The Coulombic efficiency was found to be lower with Nafion as compared to the other membranes (Figure 7).

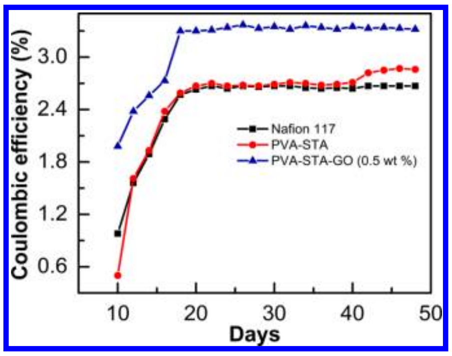

Figure 7. Comparison of Coulombic efficiency profiles of MFCs using Nafion 117, PVA–STA, and PVA–STA–GO membranes.

3.3. Effect of Membrane-Cathode-Assembly Surface Area.

Electrode assembly is a crucial aspect in microbial fuel cell design. The effect of the projected surface area of the MCA on the performance of the sMFC was studied using three different sizes (diameters), namely, 2, 3, and 4.8 cm. Enhancement in the power output was observed with increasing surface area of the MCA. When the surface area of the MCA was increased from 3.14 to 7.07 cm^2, an almost proportionate increase in the maximum power generation was observed (Figure 8). A maximum power density of 1.74 W/m^3 was achieved from the MFC with an 18.1 cm^2 projected cathode surface area, which is 61.91% and 32.67% higher than air-cathode MFCs with 3.14 and 7.07 cm^2 surface areas, respectively. The Coulombic efficiency (CE) also increased by 26.1% when the MCA surface area was increased from 3.14 cm^2 (diameter = 2 cm) to 18.1 cm^2 (diameter = 4.8 cm) and decreased by 10.63% when the cathode surface area was reduced to 7.07 cm^2. The power output using the 3.14 cm^2 MCA was found to be 49 mW/m^2, whereas with the 7.07 and 18.1 cm^2 MCA membranes, enhanced values of 85 and 128.8 mW/m^2, respectively, were achieved. An increased surface area might assist in efficient transfer of the protons from the anode chamber to the cathode chamber, thus allowing the cathodic oxygen reduction reaction to be completed at a higher rate. This experiment signifies that the reduction step in the MFC is the most critical step.[37] Although it was reported that an increase in membrane size leads to an increase in trans-membrane potential loss (membrane impedance factor), in the present study, the reverse trend was observed for the MCA area. This could be due to fact that the cathode size (along with the catalyst loading) helps more in the oxygen reduction reaction.[38] This factor dominates over the membrane impedance factor. A higher Coulombic efficiency is mainly caused by a higher current density, that is, better kinetics and/or lower resistances.

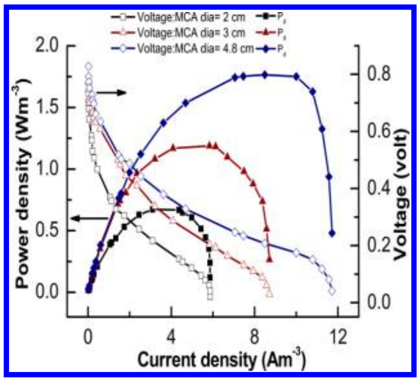

Figure 8. Comparison of polarization results for MFCs using GO-blended PVA–STA membrane-based MCAs with different diameters (2, 3, and 4.8 cm).

3.4. Effect of GO Addition to the PVA–STA Membrane.

To investigate the effect of GO incorporation on the overall performance of sMFCs in terms of power output and Coulombic efficiency, the voltage generated was monitored in three sMFCs with PVA–STA–GO membranes with GO concentrations ranging from 0.3 to 0.9 wt % (membranes M2–M4). It was found that the content of GO in the membrane significantly affected the performance of the sMFCs (Table 1). The polarization of different GO-incorporated PVA–STA–GO membranes were studied and compared with that of a native PVA–STA membrane (Figure S2, Supporting Information). The sMFC employing the PVA–STA membrane without GO

Table 1. Effects of the Addition of Different Percentages of Graphene Oxide (GO) to a PVA–STA Membrane in an Air-Cathode MFC

	graphene oxide (GO) addition to PVA–STA membrane (wt %)			
property	0 (membrane M1)	0.3 (membrane M2)	0.5 (membrane M3)	0.9 (membrane M4)
maximum open-circuit potential (mV)	734	759	788	773
maximum volumetric power density (W m^{-3})	0.81	0.97	1.48	1.19
maximum power density normalized to anode area (W m^{-2})	58.8	70.5	108	86.7
maximum Coulombic efficiency (%)	2.94	3.14	3.44	3.33
COD removal efficiency (%)	78.03	80.03	90.03	83.70
internal resistance (Ω)	154	112	87	99

produced a maximum power density of 0.80 W/m^3. Increasing the quantity of GO from 0.0 to 0.3, 0.5, and 0.9 wt % enhanced the maximum volumetric power density by 26.5%, 45.46%, and 34.6% respectively; further, increasing the GO quantity from 0.0 to 0.5 wt % improved the Coulombic efficiency by 15%. The 0.5 wt % GO-loaded PVA–STA–GO membrane exhibited higher power generation than the other two PVA–STA–GO membranes, as it had a higher conductivity than the other two. Therefore, the results suggest that the addition of GO has a fairly large influence on the Coulombic efficiency. The poor performance of the sMFC with the simple PVA–STA membrane might be due to the higher transmembrane potential loss. The anode-surface-area-normalized power density was found to be improved upon the addition of GO to the PVA–STA polymer electrolyte (Table 1). The improved power generation from the GO-impregnated membranes can be attributed to a reduction of the oxygen crossover and an increase of the proton conductivity, as well as a decrease in the internal resistance of the sMFCs. The power densities normalized to the anode surface area obtained from all four membrane-containing sMFCs (Table 1) are far higher than that recently reported (maximum 36.56 mW/m^2) by Han et al.[3] Further, it was observed that the protein content on the surface of the PVA–STA–GO membrane containing 0.5 wt % GO was much less (0.42 μg/cm^2) than the amounts on the native PVA–STA and Nafion 117 membranes (0.9 and 1.3 μg/cm^2, respectively). It has already been reported that the accumulation of these bacteria and biofoulants leads to the formation of a dense biofilm on the cation-exchange membrane (CEM) surface, resulting in greater electrical resistance. Because of their surface charges and electric motilities, most foulants move toward ion-exchange membranes, such as Nafion membranes.[38,39] Liu et al. showed that cells become flattened and lose their cellular integrity after exposure to GO dispersions. GO has a tendency to induce membrane stress on bacterial cells, resulting in the destruction of cell structures.[23] Different oxidative stress mediated by graphene-based materials was also reported, such as that mediated by reactive oxygen species. Lower amounts of biofoulant (bacterial cells and exocellular polysaccharide produced by bacteria) were found on the anolyte-facing side of the membrane with the addition of GO to the PVA–STA membrane. The overall outcome signifies that GO blending in the membrane helped enhance conductivity and reduce biofouling.

3.5. Wastewater Treatment. Wastewater treatment in sMFCs was evaluated in terms of substrate removal ability and Coulombic efficiency production. This can be explained as lower diffusion of oxygen through PVA–STA-based membranes . Substrate removal efficiency (γ) during MFC operation was evaluated using the equation

$$\gamma = \left(\frac{C_{\text{ini}} - C_{\text{final}}}{C_{\text{ini}}}\right) \times 100 \tag{5}$$

where C_{ini} represents the initial COD and C_{final} denotes final COD in the reactor.

Coulombic efficiency (CE) is a characteristic measure of the performance of MFCs. CE is the ratio between the total number of Coulombs obtained from the MFC as current to the total number of Coulombs added by the substrate. The substrate removal efficiency was found to be 91%, 83.7%, and 80.37% for sMFCs employing Nafion, PVA–STA–GO, and PVA–STA membranes, respectively. However, the Coulombic efficiency was found to be lower in the case of the Nafion membrane. This might be due to the fact that oxygen diffusion through the Nafion membrane from the cathode accounts for the loss of carbon compounds to aerobic respiration and degradation, resulting in a low CE. Coulombic efficiency is inversely proportional to COD removal. The COD removal was found to be higher in the sMFC using the Nafion membrane. This might be due to oxygen intrusion into the anode chamber and oxygen consumption due to aerobic respiration by mixed consortia including electrochemically active bacteria (EAB); the electron donation by the EAB in the anode was less than that observed in the sMFC using the PVA–STA–GO membrane. In contrast, more substrate was utilized by the EAB in the anaerobic environment in the anode chamber, as the electrons generated during respiration by the EAB in the anode were transferred efficiently in the absence of oxygen as a result of the lower diffusion of oxygen through the PVA–STA–GO-based membrane. Therefore, improved current generation and better Coulombic efficiency was achieved with PVA–STA–GO membrane.

The costs of the newly prepared membranes were calculated. It was estimated that the cost of the PVA–STA membrane was ~0.5 $/100 cm^2, whereas costs of 0.57, 0.6, and 0.61 $/100 cm^2 were estimated for the preparation of PVA–STA–GO membranes with 0.3, 0.5, and 0.9 wt % GO loadings, respectively. Commercial Nafion membranes are available for ~1.44 $/cm^2, which is 240 times costlier than the custom-made 0.5 wt % GO-blended PVA–STA–GO membrane. The results obtained in terms of power generation were compared with those from other relevant studies (Supporting Information, Table S1). The lower manufacturing costs of PVA–STA–GO composite membranes and their ability to generate high power outputs enable these membranes to be employed as promising separator materials for constructing large-scale MFCs for wastewater treatment and bioelectricity production.

4. CONCLUSIONS

Composite membranes composed of polyvinyl alcohol (PVA), silicotungstic acid (STA), and graphene oxide (GO) were prepared and evaluated as proton-conducting membranes in single-chambered microbial fuel cells (sMFCs). The synthesized PVA–STA–GO membranes showed excellent kinetic properties, better durability, and reduced oxygen crossover compared to the commercially available Nafion 117. The operating voltage was monitored along with COD removal, and the results revealed that higher volumetric power density was achieved with the PVA–STA–GO composite membranes than with a Nafion 117 membrane, mainly because of oxygen diffusion from the cathodic side to the anodic chamber, which also limits the Coulombic efficiency. GO incorporation in the PVA–STA membrane was found to have a profound influence, as it helped reduce the impedance and biofouling of the composite. Further, the power output was found to increase markedly with membrane-cathode-assembly (MCA) surface area. With the addition of GO to the membrane composite, a low-cost antifouling cation-exchange membrane (CEM) was developed with high mechanical strength and comparatively low resistance to alleviate the membrane fouling problem and, accordingly, ensure the long-term stable operation of MFCs.

ASSOCIATED CONTENT

Supporting Information

Schematic diagram of tubular sMFC, photograph of tubular sMFC, analytical measurements and calculations [power, power density, current density, and Coulombic efficiency (CE)], and polarization plot of different PVA–STA–GO membranes. Comparative study in terms of power generation using different membranes in an MFC. This material is available free of charge via the Internet at http://pubs.acs.org.

AUTHOR INFORMATION

Corresponding Author

*Tel.: +91-3222-82248/778053, +91-3222-281798. Fax: +91-3222-778707/755303. E-mail: ddas.iitkgp@gmail.com.

Author Contributions

‡S.K. and S.P. contributed equally.

Notes

The authors declare no competing financial interest.

ACKNOWLEDGMENTS

Financial support received from the Council of Scientific & Industrial Research (CSIR); University Grant Commission (UGC); Department of Biotechnology (DBT), Indian Institute of Technology Kharagpur; Bhabha Atomic Research Centre (BARC); and Ministry of New and Renewable Energy Sources (MNRE), Government of India, is duly acknowledged.

REFERENCES

(1) Wei, B.; Tokash, J. C.; Chen, G.; Hickner, M. A.; Logan, B. E. Development and Evaluation of Carbon and Binder Loading in Low-Cost Activated Carbon Cathodes for Air-Cathode Microbial Fuel Cells. *RSC Adv.* **2012**, *2*, 12751−12758.

(2) Lovley, D. R. The Microbe Electric: Conversion of Organic Matter to Electricity. *Curr. Opin. Biotechnol.* **2008**, *19*, 564−571.

(3) Han, T. H.; Khan, M. M.; Kalathil, S.; Lee, J.; Cho, M. H. Simultaneous Enhancement of Methylene Blue Degradation and Power Generation in a Microbial Fuel Cell by Gold Nanoparticles. *Ind. Eng. Chem. Res.* **2013**, *52*, 8174−8181.

(4) Kong, W.; Guo, Q.; Wang, X.; Yue, X. Electricity Generation from Wastewater Using an Anaerobic Fluidized Bed Microbial Fuel Cell. *Ind. Eng. Chem. Res.* **2011**, *50*, 12225−12232.

(5) Kalathil, S.; Lee, J.; Cho, M. H. Gold Nanoparticles Produced in Situ Mediate Bioelectricity and Hydrogen Production in a Microbial Fuel Cell by Quantized Capacitance Charging. *ChemSusChem* **2013**, *6*, 246−250.

(6) Oh, S. T.; Kim, J. R.; Premier, G. C.; Lee, T. H.; Kim, C.; Sloan, W. T. Sustainable Wastewater Treatment: How Might Microbial Fuel Cells Contribute. *Biotechnol. Adv.* **2010**, *28*, 871−881.

(7) Kim, B. H.; Chang, I. S.; Gadd, G. M. Challenges in Microbial Fuel Cell Development and Operation. *Appl. Microbiol. Biotechnol.* **2007**, *76*, 485−494.

(8) Watanabe, K. Recent Developments in Microbial Fuel Cell Technologies for Sustainable Bioenergy. *J. Biosci. Bioeng.* **2008**, *106*, 528−536.

(9) Li, W.-W.; Sheng, G.-P.; Liu, X.-W.; Yu, H.-Q. Recent Advances in the Separators for Microbial Fuel Cells. *Bioresour. Technol.* **2011**, *102*, 244−252.

(10) Fan, Y.; Hu, H.; Liu, H. Enhanced Coulombic Efficiency and Power Density of Air-Cathode Microbial Fuel Cells with an Improved Cell Configuration. *J. Power Sources* **2007**, *171*, 348−354.

(11) Ayyaru, S.; Letchoumanane, P.; Dharmalingam, S.; Stanislaus, A. R. Performance of Sulfonated Polystyrene−Ethylene−Butylene−Polystyrene Membrane in Microbial Fuel Cell for Bioelectricity Production. *J. Power Sources* **2012**, *217*, 204−208.

(12) Cropper, M. A.; Geiger, S.; Jollie, D. M. Fuel Cells: A Survey of Current Developments. *J. Power Sources* **2004**, *131*, 57−61.

(13) Kim, J. R.; Cheng, S.; Oh, S.-E.; Logan, B. E. Power Generation Using Different Cation, Anion, and Ultrafiltration Membranes in Microbial Fuel Cells. *Environ. Sci. Technol.* **2007**, *41*, 1004−1009.

(14) Choi, M.-J.; Chae, K.-J.; Ajayi, F. F.; Kim, K.-Y.; Yu, H.-W.; Kim, C.; Kim, I. S. Effects of Biofouling on Ion Transport through Cation Exchange Membranes and Microbial Fuel Cell Performance. *Bioresour. Technol.* **2011**, *102*, 298−303.

(15) Ayyaru, S.; Dharmalingam, S.; Ayyaru, S.; Dharmalingam, S. Development of MFC Using Sulphonated Polyether Ether Ketone (SPEEK) Membrane for Electricity Generation from Waste Water. *Bioresour. Technol.* **2011**, *102*, 11167−11171.

(16) Peighambardoust, S. J.; Rowshanzamir, S.; Amjadi, M. Review of the Proton Exchange Membranes for Fuel Cell Applications. *Int. J. Hydrogen Energy* **2010**, *35*, 9349−9384.

(17) Zhang, Q. G.; Liu, Q. L.; Chen, Y.; Chen, J. H. Dehydration of Isopropanol by Novel Poly(vinyl alcohol)−Silicone Hybrid Membranes. *Ind. Eng. Chem. Res.* **2007**, *46*, 913−920.

(18) Anis, A.; Banthia, A. K.; Bandyopadhyay, S. Synthesis & Characterization of PVA/STA Composite Polymer Electrolyte Membranes for Fuel Cell Application. *J. Mater. Eng. Perform.* **2008**, *17*, 772−779.

(19) Shanmugam, S.; Viswanathan, B.; Varadarajan, T. K. Synthesis and Characterization of Silicotungstic Acid Based Organic−Inorganic Nanocomposite Membrane. *J. Membr. Sci.* **2006**, *275*, 105−109.

(20) Tseng, C.-Y.; Ye, Y.-S.; Cheng, M.-Y.; Kao, K.-Y.; Shen, W.-C.; Rick, J.; Chen, J.-C.; Hwang, B.-J. Sulfonated Polyimide Proton Exchange Membranes with Graphene Oxide Show Improved Proton Conductivity, Methanol Crossover Impedance, and Mechanical Properties. *Adv. Energy Mater.* **2011**, *1*, 1220−1224.

(21) Krishnan, D.; Kim, F.; Luo, J.; Cruz-Silva, R.; Cote, L. J.; Jang, H. D.; Huang, J. Energetic Graphene Oxide: Challenges and Opportunities. *Nano Today* **2012**, *7*, 137−152.

(22) Bai, H.; Sheng, K.; Zhang, P.; Li, C.; Shi, G. Graphene Oxide/Conducting Polymer Composite Hydrogels. *J. Mater. Chem.* **2011**, *21*, 18653−18658.

(23) Liu, S.; Zeng, T. H.; Hofmann, M.; Burcombe, E.; Wei, J.; Jiang, R.; Kong, J.; Chen, Y. Antibacterial Activity of Graphite, Graphite Oxide, Graphene Oxide, and Reduced Graphene Oxide: Membrane and Oxidative Stress. *ACS Nano* **2011**, *5*, 6971−6980.

(24) Hummers, W. S.; Offeman, R. E. Preparation of Graphitic Oxide. *J. Am. Chem. Soc.* **1958**, *80*, 1339.

(25) Behera, M.; Jana, P. S.; Ghangrekar, M. M. Performance Evaluation of Low Cost Microbial Fuel Cell Fabricated Using Earthen Pot with Biotic and Abiotic Cathode. *Bioresour. Technol.* **2010**, *101*, 1183−1189.

(26) Lefebvre, O.; Shen, Y.; Tan, Z.; Uzabiaga, A.; Chang, I. S.; Ng, H. Y. A Comparison of Membranes and Enrichment Strategies for Microbial Fuel Cells. *Bioresour. Technol.* **2011**, *102*, 6291−6294.

(27) Aelterman, P.; Rabaey, K.; Pham, H. T.; Boon, N.; Verstraete, W. Continuous Electricity Generation at High Voltages and Currents Using Stacked Microbial Fuel Cells. *Environ. Sci. Technol.* **2006**, *40*, 3388−3394.

(28) Lowry, O. H.; Rosebrough, N. J.; Farr, A. L.; Randall, R. J. Protein Measurement with the Folin Phenol Reagent. *J. Biol. Chem.* **1951**, *193*, 265−275.

(29) Murphy, D. J.; Prinsley, R. T. Interaction of Triton X-100 with the Pigment−Protein Complexes of Photosynthetic Membranes. *Biochem. J.* **1985**, *229*, 31−37.

(30) Gonçalves, G.; Marques, P. A. A. P.; Barros-Timmons, A.; Bdkin, I.; Singh, M. K.; Emami, N.; Grácio, J. Graphene Oxide Modified with PMMA via ATRP as a Reinforcement Filler. *J. Mater. Chem.* **2010**, *20*, 9927−9934.

(31) Mansur, H. S.; Sadahira, C. M.; Souza, A. N.; Mansur, A. A. P. FTIR Spectroscopy Characterization of Poly(vinyl alcohol) Hydrogel with Different Hydrolysis Degree and Chemically Crosslinked with Glutaraldehyde. *Mater. Sci. Eng. C* **2008**, *28*, 539−548.

(32) Fu, Y.; Chen, Q.; He, M.; Wan, Y.; Sun, X.; Xia, H.; Wang, X. Copper Ferrite−Graphene Hybrid: A Multifunctional Heteroarchitecture for Photocatalysis and Energy Storage. *Ind. Eng. Chem. Res.* **2012**, *51*, 11700−11709.

(33) Yang, C.-C. Synthesis and Characterization of the Cross-Linked PVA/TiO_2 Composite Polymer Membrane for Alkaline DMFC. *J. Membr. Sci.* **2007**, *288*, 51−60.

(34) Bai, H.; Li, C.; Wang, X.; Shi, G. A pH-Sensitive Graphene Oxide Composite Hydrogel. *Chem. Commun.* **2010**, *46*, 2376−2378.

(35) Wang, F.; Hickner, M.; Kim, Y. S.; Zawodzinski, T. A.; McGrath, J. E. Direct Polymerization of Sulfonated Poly(arylene ether sulfone) Random (Statistical) Copolymers: Candidates for New Proton Exchange Membranes. *J. Membr. Sci.* **2002**, *197*, 231−242.

(36) Kim, H. M.; Lee, J. K.; Lee, H. S. Transparent and High Gas Barrier Films Based on Poly(vinyl alcohol)/Graphene Oxide Composites. *Thin Solid Films* **2011**, *519*, 7766−7771.

(37) Pandit, S.; Ghosh, S.; Ghangrekar, M. M.; Das, D. Performance of an Anion Exchange Membrane in Association with Cathodic Parameters in a Dual Chamber Microbial Fuel Cell. *Int. J. Hydrogen Energy* **2012**, *37*, 9383−9392.

(38) Khilari, S.; Pandit, S.; Ghangrekar, M. M.; Das, D.; Pradhan, D. Graphene Supported α-MnO_2 Nanotubes As a Cathode Catalyst for Improved Power Generation and Wastewater Treatment in Single-Chambered Microbial Fuel Cells. *RSC Adv.* **2013**, *3*, 7902−7911.

(39) Bellona, C.; Drewes, J. E.; Xu, P.; Amy, G. Factors Affecting the Rejection of Organic Solutes during NF/RO Treatment—A Literature Review. *Water Res.* **2004**, *38*, 2795−2809.